MULTISOURCE AND MULTITEMPORAL LAND COVER MAPPING OF GREATER LUZON ISLAND USING GOOGLE EARTH ENGINE

C. G. Candido[1,2*], A. C. Blanco[1,2], N. J. B. Borlongan[1], R. M. de la Cruz[1]

[1] Space Information and Infrastructure Bureau, Philippine Space Agency, Quezon City 1109, Philippines – christian.candido@philsa.gov.ph, noel.borlongan@philsa.gov.ph, roel.delacruz@philsa.gov.ph
[2] Department of Geodetic Engineering, University of the Philippines Diliman, Quezon City- acblanco@up.edu.ph

KEY WORDS: Classification, Sentinel-2, Landsat-8, Harmonization, Google Earth Engine, Google Colaboratory, Random Forest

ABSTRACT:

A variety of research endeavors and practical applications necessitate the use of land cover maps. These maps are valuable for tasks such as change detection, forest monitoring, urban expansion monitoring, natural resource mapping, catering to diverse user requirements. While satellite sensors offer essential data for comprehending spatial and temporal variations in land cover, relying on a single satellite system can be limiting, especially considering the potential hindrance of cloud cover in the case of optical sensors. To enhance temporal frequency, it becomes essential to utilize multiple satellite systems, albeit requiring harmonization to ensure consistent outcomes. This study presents a large-scale annual land cover mapping which utilizes harmonized Landsat-8 and Sentinel-2 satellite imagery, in conjunction with supplementary data, and a machine learning algorithm. In addition, the use of powerful computational processing platforms such as Google Earth Engine and Google Colaboratory is now a requirement to manage big geospatial data as well as to run different algorithms for processing and analysis.

1. INTRODUCTION

The rapid and wide-ranging changes in land use/land cover patterns caused by the rapid increase in population, expansion of urban areas, continuous land use/land cover transformation, and widespread deforestation has led to the emergence of numerous environmental issues with adverse effects on the ecosystem and biodiversity. With the rapid alteration of land cover, accurate and frequent monitoring and mapping of land cover patterns becomes an essential part of policymaking with regards to sustainable development and natural resource management (Ma et. Al., 2015). For the monitoring and mapping of land cover, remote sensing techniques have been widely used, in part due to the increasing availability of different Earth Observation (EO) data.

The wide availability of EO data acquired through satellite sensors has provided the necessary data for monitoring and understanding spectral, spatial, and temporal variation in land cover patterns (Wang, et. Al., 2017). Given the improved spatial and temporal capabilities of contemporary satellite sensors, substantial amounts of remotely sensed data need to be processed, analyzed, and visualized. The advancements in the capability of satellite sensors have shifted the focus of land cover mapping to the use of geospatial big data and powerful computing systems and platforms. Robust and powerful computational processing capacities are now a requirement to manage big geospatial data as well as to run different algorithms for processing and analysis (Pratico, et. Al., 2021).

Gomez et al. (2016) emphasized the importance of accurate and frequent monitoring for effective policymaking. Satellite sensors provide the necessary data to understand spatial and temporal variations in land cover patterns (Wang et al., 2017). However, the volume of data generated requires advanced processing capabilities. Cloud-based computation platforms like Google Earth Engine (GEE) have emerged as a solution, offering the ability to process and analyze large geospatial datasets. GEE employs Google's cloud infrastructure and JavaScript-based language for geospatial data processing (Luo et al., 2021; Hird et al., 2020). Numerous studies have demonstrated GEE's effectiveness in mapping various land cover types at different scales (Zhang et al., 2020). In a study conducted by Hird, et. al. (2017), a workflow for predicting the probability of wetlands on a regional scale was created using the GEE and R Statistical Software.

Global land cover datasets have become available and released publicly. In 2021, ESRI partnered with Impact Observatory and Microsoft to release a 10-meter Land Use/Land Cover (LULC) map for 2020 generated through artificial intelligence (AI) techniques, utilizing European Space Agency (ESA) Sentinel-2 imagery. Additionally, in the same year, the European Space Agency (ESA) released the World Cover map, a global land cover map for 2020, with a 10-meter resolution derived from both Sentinel-1 and Sentinel-2 satellites. Following favorable feedback from users, ESA decided to enhance the World Cover project by creating a new, higher quality version for the year 2021 which was made available in 2022. Also in the same year, Google, in collaboration with the World Resources Institute, introduced Dynamic World, a 10-meter near-real-time (NRT) global land use land cover dataset created using deep learning techniques. These global land cover datasets are released under a Creative Commons license which means that the datasets are provided free of charge, without restriction of use. While these datasets are free for all to use, the training datasets used to create these products are also global in coverage, which means that there are instances where inaccuracies will be present in areas which were not captured by their training datasets.

In the Philippines, a national land cover maps are released by the National Mapping and Resource Information Authority (NAMRIA) every 5 years. However, many different applications and studies require more frequent land cover

* Corresponding author

updates, such as agriculture monitoring, emerging settlements, urban sprawl monitoring, forest monitoring and detection of deforestation activities, and mangrove mapping, among others. Considering the potential benefits offered by geospatial big data, cloud-based computational platform, and multisource data might have for large-scale, reliable, and frequent land cover mapping and monitoring, the objective of this study is to use a machine learning algorithm for large-scale mapping of land cover though the use of cloud-based computation platform, Google Earth Engine, and Google Colaboratory. The study entails generating an accurate land cover classification map encompassing the Greater Luzon Island. Landsat 8 OLI and Sentinel 2 was used to derived phenological features and composites of spectral bands and band indices which was then used alongside topographic features (DEM, slope, topographic diversity) and night-time lights to classify the selected land cover categories in the Luzon Island.

2. STUDY AREA

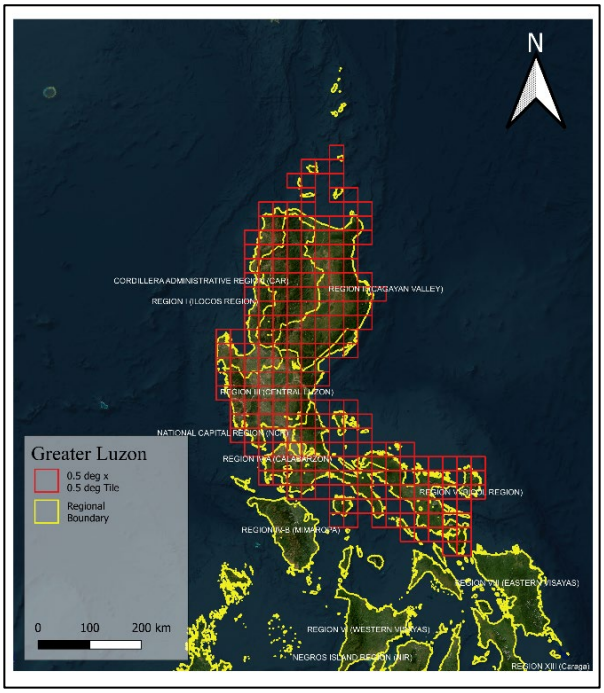

Figure 1. Geographic location of Greater Luzon Island overlaid with 0.5 x 0.5 degrees tiles.

The area for this study is the Greater Luzon Island (GLI) (shown in Figure 1). It is the largest island in the Philippines that covers seven regions, i.e., Region 1 (Ilocos Region), Region 2 (Cagayan Valley), Region 3 (Central Luzon), Region 4A (CALABARZON), Region 5 (Bicol), Cordillera Administrative Region (CAR), and the National Capital Region (NCR). The Greater Luzon Island measures around 104,688 square kilometers and is roughly oriented with its longest axis north to south from 18°32' N to 12°31' N.

Since the whole island covers a very large area, the processing of the whole island in Google Earth Engine cannot be done without experiencing memory limitations. Thus, a grid of 0.5 x 0.5 degrees tiles was created wherein the generation of land cover classification images will be done per tile and the results can be mosaicked afterwards.

3. METHODOLOGY

The proposed methodology for classifying land cover types of Greater Luzon Island is outlined through the following worklows: Landsat-Sentinel harmonization, feature and machine learning algorithm selection, model training and validation, and post-classification. The overall methodology is shown in Figure 3 and Figure 4.

3.1 Landsat-Sentinel Harmonization

Landsat 8 (L8) was launched by NASA in 2013 and is presently operating alongside Landsat 7 (L7). The joint utilization of L7 and L8 generates three to four observations per month. Since 2015, Sentinel 2 (S2) constellation from the European Space Agency (ESA) has been delivering global scale imagery with a revising time of 5 to 10-day at resolutions ranging from 10 to 60 m. The proven compatibility between the L7, L8 and S2 bands provides the opportunity for monitoring at near-daily medium resolution by merging their observations (Nguyen et al., 2020). By harmonizing the Landsat and Sentinel observations, the temporal frequency of observations can be increased, and more insights can be gathered in the areas of interest. Harmonization can also help in cloud-infested areas, creating more opportunities for observations. Nevertheless, synthesizing (or harmonizing) L7, L8 and S2 is still a challenging process that requires several steps.

The harmonization process used in this study is based on the work of Nguyen et al. 2020 entitled "Harmonization of Landsat and Sentinel 2 for Crop Monitoring in Drought Prone Areas: Case Studies of Ninh Thuan (Vietnam) and Bekaa (Lebanon)". The harmonization process is composed of the following procedures: image selection, atmospheric correction, cloud and cloud shadows masking, BRDF and topographic correction, band adjustment, resampling, and reprojection. Atmospheric correction is implemented in Jupyter notebook while the rest of the steps are done in Google Earth Engine.

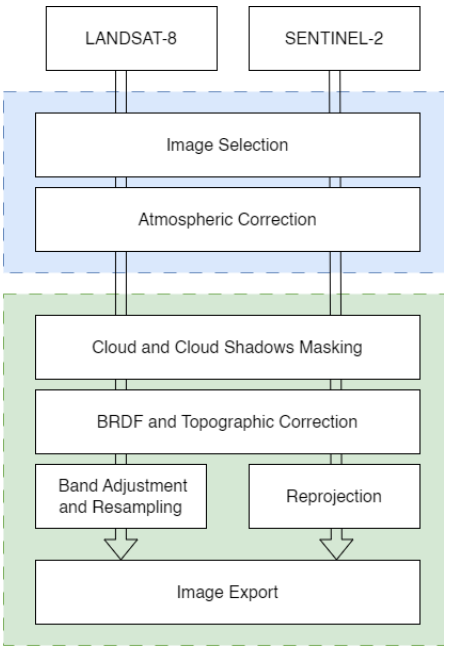

Figure 2. Modified Landsat-Sentinel harmonization workflow based on the work of Nguyen et al. (2020) The steps inside the blue region can be done in Jupyter Notebook while those inside the green region can be done in Google Earth Engine.

3.1.1 Image selection

The image selection step filters the image collections and selects images based on location, date range, and cloud percentage cover specified by the user.

3.1.2 Atmospheric Correction

Atmospheric correction corrects the images and converts the sensor radiance to a quantity more closely related to the properties of the target, such as ground reflectance or emissivity. This step may be skipped if the images selected by the user are already atmospherically corrected.

3.1.3 Clouds and Cloud Shadows Masking

Clouds and cloud shadows are masked from the images to remove these unwanted pixels. Available techniques for cloud masking are using the cloud mask QA band, using a cloud score, and using random forest classifier to train cloud and cloud shadow pixels detection and masking.

3.1.4 BRDF and Topographic Correction

Landsat and Sentinel-2 satellites acquire images at view angles ±7.5° and ±10.3° respectively from nadir that cause small directional effects in the surface reflectance. The solar zenith angle can also vary over the year which can cause changes in the reflectance values even if the surface remains the same. These effects are described by the bidirectional reflectance distribution function (BRDF) and should be minimized to harmonize both Landsat and Sentinel-2 datasets for reliable and consistent data.

Topography can also contribute to differences in surface reflectance of similar land cover. Topographic correction should be considered especially for terrains with varying elevations and slope such as mountains or rugged terrains.

3.1.5 Band Adjustment

Both Landsat and Sentinel-2 missions have radiometric and geometric calibration algorithms of their own to maintain quality and interoperability of their datasets. However, small spectral differences exist in the bands of the Landsat and Sentinel-2 missions. Hence, there is a need to adjust the values of the Landsat bands to match the values of the Sentinel-2 bands (or vice versa). The adjustment is in the form of transformation coefficients.

3.1.6 Resampling and Reprojection

A harmonized dataset should have uniform spatial resolution and projection across all bands. Landsat datasets have 30m resolution and WGS84 geographic projection. Sentinel-2 datasets have 10m resolution and Universal Transverse Mercator (UTM) projection. In this study, Landsat datasets are resampled to 10m resolution and Sentinel-2 datasets are reprojected to WGS84 geographic projection to have a uniform spatial resolution and projection across all datasets and bands.

3.2 Feature Dataset Preparation

The land cover classification of GLI was generated using the harmonized data of L8 OLI and S2 Level-2A Imageries acquired from January 2022 to December 2022 using freely available datasets in GEE. Satellite images with less than 30.0% cloud cover were queried from the image collection, compiled into one year composite, and harmonized. In addition, the compiled image collection was used to extract phenological features using Harmonic Regression and different band indices of the 12 land cover types. The pre-processing and extraction of features were done in the Google Colaboratory Environment using different Python packages including the Earth Engine API and Geemap (Luo et. al, 2021). The table below shows the list of features that were extracted from the image collection of harmonized Landsat 8 and Sentinel-2 data.

After the features were extracted from the harmonized image collection of L8 and S2, they were aggregated and reduced into one composite. Additional features such as nighttime lights (from Visible Infrared Imaging Radiometer Suite), digital elevation model, and slope were then added in the dataset to form the image classification features.

Features	Type of Features
NDVI, NDBI, NDWI, SAVI, MVI	Spectral Indices Features
Phase, Amplitude, Mean EVI, Median EVI, Max EVI, Min EVI, Std Dev EVI	Phenological Features
Blue, Green, Red, NIR, SWIR 1, SWIR 2	Spectral Band Features

Table 1. Features extracted from the harmonized data of Sentinel-2 and Landsat 8 satellite imageries

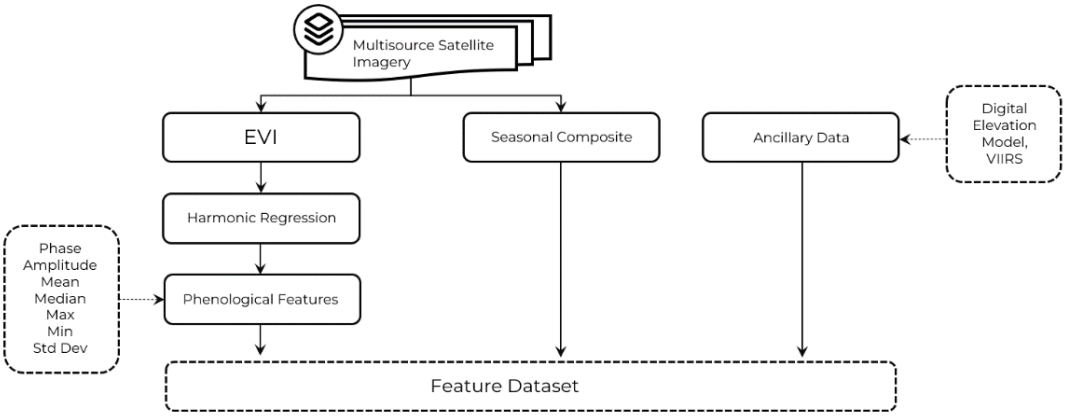

Figure 3. First part of the proposed methodology for land cover mapping covering feature dataset preparation

Land cover	Description
Annual Crop	Includes bare soil of cultivated land, harvested arable crops (maize, corn, sugarcane) except rice
Aquaculture	Farming of aquatic organisms in both coastal and inland areas
Barren Land	Land with little or no layers of vegetation cover
Dense Urban	Urban structures and transport networks are dominating the surface area (>70%). Includes urban center types and dense suburbs where buildings form a continuous and homogenous fabric
Forest	Land with an area of more than 0.5 hectares and tree crown cover of more than 10%. The trees should be able to reach a minimum height of 5 meters at maturity.
Grassland	Are predominantly vegetated with grasses such as Imperata, Themada, Saccharum spp., among others
Mangrove	Forested wetland growing along tidal mudflats and along shallow water coastal areas extending inland along rivers, streams, and their tributaries
Paddy Rice	Flooded field of arable land used to cultivate rice (separated from annual crop)
Permanent Crop	Crops that are considered permanent such as fruit trees (mango, kalamansi, etc.), some herbaceous plants (bananas), stemless plants (pineapples)
Shrubland	Land dominated by woody vegetation which are generally more than 0.5 meter and less than 5.0 meters in height and without a definite crown
Mixed Urban	Associated vegetated areas and bare surface areas are present and occupy significant portion in urban structures and transport networks.
Water	Open ocean and seas, streams, rivers, lakes, and other inland body of water

Table 2. The 12 land cover types used in this study.

3.2 Reference Data Annotation

A rigorous manual annotation procedure was employed to create reference datasets, which were subsequently divided into three independent datasets namely: one for training, one for test, and one for validation procedure. Given the significance of representative samples in supervised classification, a thorough examination of the study area was conducted. Different secondary data sources, such as Google Earth Images, NAMRIA Land Cover Maps, Drone Data, and OpenStreetMap data were used for interpretation and manual annotation of different land cover types. Taking into consideration the NAMRIA Land Cover classification and the complex landscape of the study area, a total of 12 land cover classes were manually identified and annotated: (1) Annual Crop, (2) Aquaculture, (3) Barren Land, (4) Dense Urban, (5) Forest, (6) Grassland, (7) Mangrove/Wetland, (8) Paddy Rice, (9) Permanent Crop, (10) Shrubland, (11) Mixed Urban, and (12) Water.

3.3 Predicting Land cover using Random Forest Algorithm

A supervised classification was then performed on the feature dataset to produce the classified image of GLI. Random forest was used as the machine learning algorithm for the classification procedure. Random Forest is a supervised machine learning algorithm that builds an ensemble of decision trees and merges them together usually by bootstrapping method to get a more accurate and stable prediction. Random forest was chosen because of its high efficiency in handling big data and its ability to reduce overfitting compared to other machine learning algorithms available in Google Earth Engine Platform such as Support Vector Machine, Naïve Bayes, or CART (Belgiu & Dragut, 2014). Prior to the classification procedure, the hyperparameters of the Random Forest were fine-tuned using the "fit" and "score" method. This involved fitting the model with a set of hyperparameters to the training dataset and evaluating the score of the model using the test dataset. This fitting and evaluation process is iteratively repeated until the optimal hyperparamaters are identified. After determining the best set of hyperparameters, the Random Forest was then implemented on the feature dataset for the classification (Pedregosa, et. al., 2011).

3.4 Accuracy Assessment

Among the crucial final steps of every classification procedure is accuracy assessment. The aim of accuracy assessment is to quantitatively evaluate how efficiently the pixels were sampled into the correct land cover classes. Field data from ODK and Drone Images, SkySat Scene Product, and Google Earth Images were used to generate a total of 301 random points (shown on figure 5). Determination of the random points is carried out to identify the area that represents each desired land cover class.

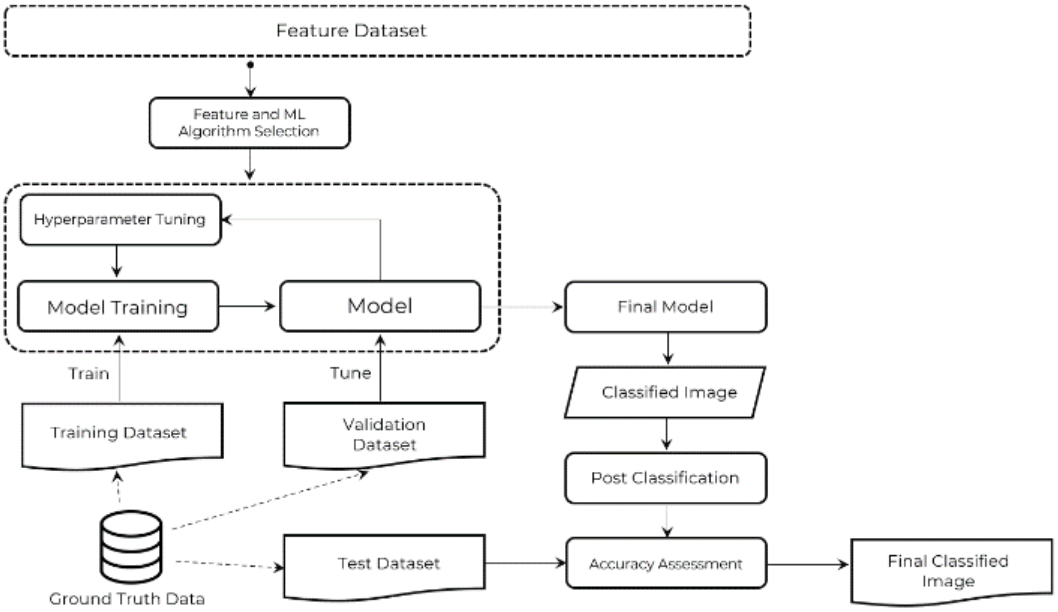

Figure 4. Second part of the methodology for land cover mapping covering supervised classification

The most widely prompted classification accuracy is in the form of confusion matrix. Descriptive and analytical statistics could be derived from this confusion matrix. In this study, various evaluation metrics related with classification accuracy were computed based on the formulation as indicated below:

$$Overall\ Accuracy\ (OA) = \frac{TP+TN}{TP+TN+FP+FN} \quad (1)$$

$$Kappa = \frac{2*(TP*TN-FN*FP)}{(TP+FP)*(FP+TN)+(TP+FN)*(FN+TN)} \quad (2)$$

$$Precision = \frac{TP}{TP+FP} \quad (3)$$

$$Recall = \frac{TP}{TP+FN} \quad (4)$$

$$F1-score = \frac{2\ x\ Precision\ x\ Recall}{Precision+Recall} \quad (5)$$

Where TP is True Positives which are number of samples correctly predicted as "positive", FP is False Positives which are number of samples wrongly predicted as "positive", TN is True Negatives which are number of samples correctly predicted as "negative", and lastly FN is False Negatives which are samples wrongly predicted as "negative".

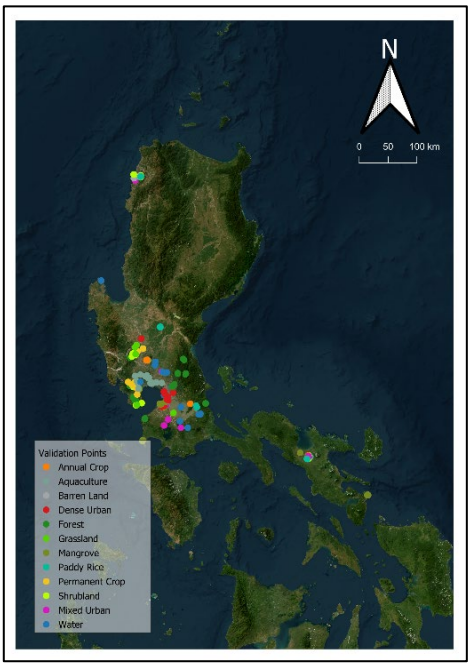

Figure 5. Validation points generated from variety of datasets (ODK, Drone data, SkySat Scene, and Google Earth Images)

4. RESULTS AND DISCUSSION

Figure 6 shows the land cover classification result of Random Forest classifier for the harmonized L8 and S2 data and the derived spectral indices, phenological features, and ancillary dataset implemented on GEE and Google Colaboratory Environment. The classified image of Greater Luzon Island underwent an accuracy assessment, involving the generation of confusion matrix with standard measures of accuracy (overall accuracy, kappa coefficient, recall, precision, and F1-score). Table 3 shows the result of the per-class accuracy assessment (recall, precision, and F1-score) for 2022 land cover map.

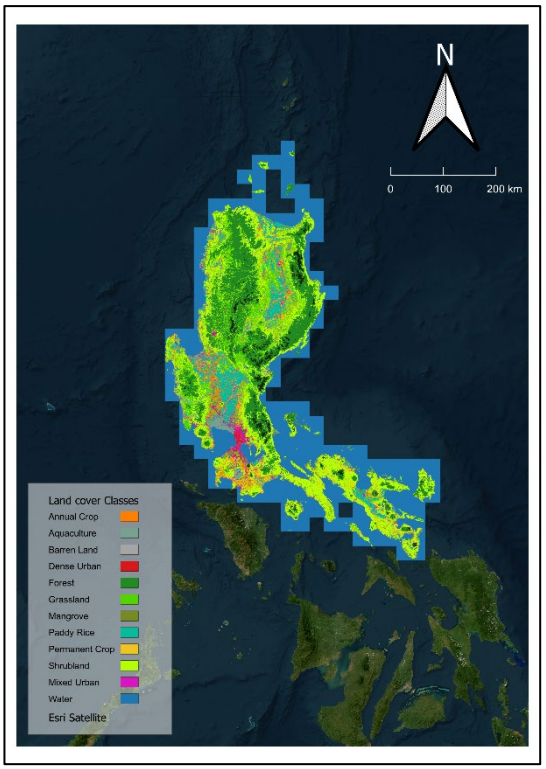

Figure 6. 2022 Land cover classification of Greater Luzon Island produced using Google Earth Engine and Google Colaboratory Platform

Results of the accuracy assessment reveal an overall accuracy of 81.6% and a kappa coefficient of 0.80. Class-specific precision and recall exhibit a range from 57.7% (in the case of the grassland class) to 100.0% (for the mangrove and mixed urban classes). Notably, the mangrove class attains the highest F1-score, reaching 96.6%, while the shrubland class registers the lowest F1-score at 66.7%. This broad spectrum of accuracy values underscores significant confusion between land cover classes specifically the grassland, and shrubland.

Land cover class	F1-score	Recall	Precision
Annual crop	88.0	76.9	83.3
Aquaculture	88.2	88.2	88.2
Barren land	71.4	80.0	64.5
Dense Urban	96.2	100.0	92.6
Forest	86.4	82.6	90.5
Grassland	69.8	88.2	57.7
Mangrove	96.6	93.3	100.0
Paddy Rice	87.5	97.2	79.5
Permanent Crop	71.8	66.7	77.8
Shrubland	66.7	59.5	75.9
Mixed Urban	85.1	74.1	100.0
Water	90.9	88.2	93.8

Table 3. Per-class accuracy metrics of the land cover generated using Random Forest Algorithm classifier. The F1-score, recall, and precision were computed for the 2022 land cover produced.

Furthermore, the low precision, as evidenced by the grassland class's 57.7%, signifies an excessive rate of false positives produced by the classifier. This suggests an overestimation of the true grassland land cover class, as many areas have been erroneously classified as grassland. Examining the confusion matrix (Figure 7), it is evident that numerous areas designated as annual crop and a smaller number of areas categorized as barren land, permanent crop, and mixed urban were inaccurately classified as grassland. This confusion between grassland and annual crop may be attributed to their similar spectral and spatial characteristics.

Conversely, the shrubland class exhibits a low recall, implying that the classifier generates a substantial number of false negatives for this land cover category. Many regions designated as shrubland are not classified as such but are instead categorized as other land cover types, particularly barren land, paddy rice, and permanent crop. Several factors may contribute to the classifier's inability to correctly classify shrubland, including potential changes in land cover over time. Shrublands are susceptible to alterations due to utilization or conversion into alternative land cover or land use practices.

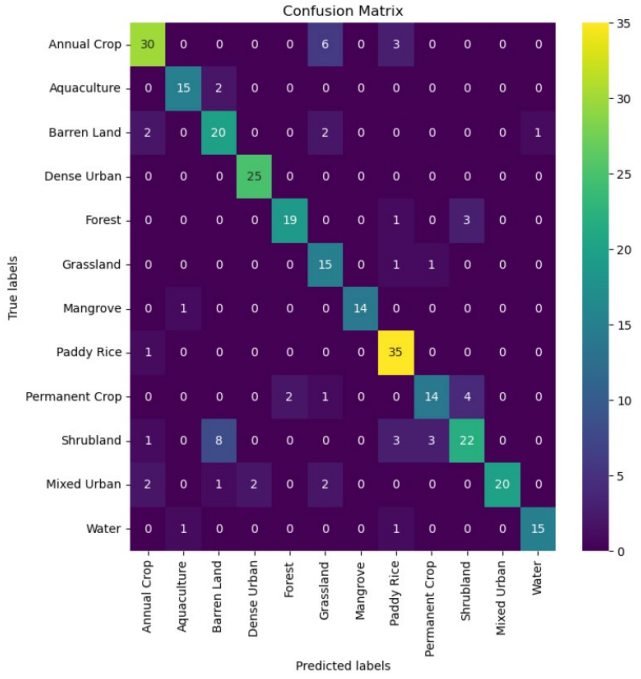

Figure 7. Generated confusion matrix of the trained random forest classifier

5. CONCLUSION

In this study, we introduce a methodology for large-scale land cover mapping using the combination of Google Earth Engine Platform and Google Colaboratory Environment, which leverages multisource and multitemporal satellite images. The primary objective of this methodology is to generate a comprehensive land cover map for Greater Luzon Island, derived from a time-series of harmonized Landsat 8 and Sentinel 2 satellite imagery, while employing the Google Earth Engine Platform and Google Colaboratory Environment.

To achieve this, the proponents utilized the Random Forest classifier, selected for its robustness in handling big geospatial data. The generated land cover map demonstrated an overall accuracy of 81.6% and a kappa coefficient of 0.80. These results indicate favorable criteria, rendering them suitable for further analysis. Additionally, we computed F1-scores, precision, and recall for various land cover classes, as individual accuracy assessment parameters, which provide valuable insights into the model's performance concerning specific categories or classes.

REFERENCES

Belgiu, M., Drăgut, L., 2014. Comparing supervised and unsupervised multiresolution segmentation approaches for extracting buildings from very high-resolution imagery. *ISPRS Journal Photogrammetry Remote Sens*ing, 96, 67–75.

Gomez, C., White, J. C., and Wulder, M. A., 2016. Optically Remotely Sensed Time Series Data for Land Cover Classification: A Review. *ISPRS Journal of Photogrammetry and Remote Sensing*, 116, 55-72.

Hird, J., DeLancey, E., McDermid, G., and Kariyeva, J., 2017. Google Earth Engine, Open-Access Satellite Data, and Machine Learning in Support of Large-Area Probabilistic Wetland Mapping. *Remote Sensing*, 9, 1315

Luo, C., Qi, B., Liu, H., Guo, D., Lu, L., Fu, Q., and Shao, S., 2021. Using Time Series Sentinel-1 Images for Object-Oriented Crop Classification in Google Earth Engine, *Remote Sensing*, 13, 561

Ma, Y., Wu, H., Wang, L., Huang, B., Ranjan, R., Zomaya, A.Y., Jie, W., 2015. Remote sensing big data computing: Challenges and opportunities. *Future Generation Computing System*, 51, 47–60.

Pedregosa, F., Varoquaux, G., Gramfort, A., Michel, V., Thirion, B., Grisel, O., Blondel, M., Prettenhoffer, P., Weiss, R., Dubourg, V., Vanderplas, J., Passos, A., Cournapeau, D., Brucher, M., Perrot, M., and Duchesnay, E., 2011. Scikit learn: Machine Learning in Python, *Journal of Machine Learning Research*, 12, 2825-2830

Pratico, S., Solano, F., Di Fiazo, S., and Modica, G., 2021. Machine Learning Classification of Mediterranean Forest Habitats in Google Earth Engine Based on Seasonal Sentinel-2 Time-Series and Input Composition Optimisation. *Remote Sensing*, 12, 586

Wang, Z., Lin, C.H., 2017. Pseudo Invariant Features Selection for Optical Satellite Images using Multitemporal and Multivariate Alteration Detection, master's Thesis, National Cheng Kung University, No. 1, Dasyue Rd, East District, Tainan City, Taiwan 701

Zhang, H., Eziz, A., Xiao, J., Tao, S., Wang, S., Tang, Z., Zhu, J., and Fang, J., 2019. High-Resolution Vegetation Mapping using eXtreme Gradient Boosting Machine based on Extensive Features. *Remote Sensing*, 11, 1505

Nguyen, M.D., Baez-Villanueva, O.M., Bui, D.D., Nguyen, P.T., Ribbe, L., 2020. Harmonization of Landsat and Sentinel 2 for Crop Monitoring in Drought Prone Areas: Case Studies of Ninh Thuan (Vietnam) and Bekaa (Lebanon). *Remote Sensing*, 12, 281

Colby, J.D., 1991. Topographic normalization in rugged terrain. *Photogrammetry Eng. Remote Sens.*, 57, 531–537

Claverie, M., Ju, J., Masek, J.G., Dungan, J.L., Vermote, E.F.,

Roger, J. C., Skakun, S.V., Justice, C., 2018. The Harmonized Landsat and Sentinel-2 surface reflectance data set. *Remote Sensing of Environment*, 219, 145–161

Barsi, J.A., Alhammoud, B., Czapla-Myers, J., Gascon, F., Haque, M.O., Kaewmanee, M., Leigh, L., Markham, B.L., 2018. Sentinel-2A MSI and Landsat-8 OLI radiometric cross comparison over desert sites. *European Journal of Remote Sensing*, 51, 822–837

Chastain, R., Housman, I., Goldstein, J., Finco, M., Tenneson, K., 2019. Empirical cross sensor comparison of Sentinel-2A and 2B MSI, Landsat-8 OLI, and Landsat-7 ETM+ top of atmosphere spectral characteristics over the conterminous United States. *Remote Sensing of Environment*, 221, 274–285